ACS OMEGA

http://pubs.acs.org/journal/acsodf

Article

Synthesis, Characterization, and DFT-Based Electronic and Nonlinear Optical Properties of Methyl 1-(arylsulfonyl)-2-aryl-1H-benzo[d]imidazole-6-carboxylates

Shumaila Aslam, Muhammad Haroon, Tashfeen Akhtar,* Muhammad Arshad, Muhammad Khalid,* Zahid Shafiq, Muhammad Imran, and Aman Ullah*

Cite This: *ACS Omega* 2022, 7, 31036−31046

Read Online

ACCESS | Metrics & More | Article Recommendations | Supporting Information

ABSTRACT: Herein, a series of *N*-1-sulfonyl substituted derivatives of 2-substituted benzimidazoles (**2a−2e**) were designed and synthesized via structural tailoring of the acceptor part of donor−π−acceptor schemes, and their nonlinear optic (NLO) characteristics were reported. The structures of **2a−2e** were investigated and their characterization was accomplished by employing spectroscopic procedures, *i.e.*, UV−vis, FT-IR, and ^{1}H and ^{13}C NMR. Further, a density functional theory (DFT) approach was used to calculate UV−vis, vibrational, and ^{1}H and ^{13}C NMR techniques; frontier molecular orbitals (FMOs); global reactivity parameters (GRPs); natural bond orbitals (NBOs); optical and vibrational analysis; and nonlinear optics (NLO). The most promising results were obtained for 6-nitro-2-(4-nitrophenyl)-1-(4-nitrophenylsulfonyl)-1*H*-benzo[*d*]imidazole among entitled compounds, as it exhibited the highest $\langle\alpha\rangle$ and β_{tot} values, showing it is an eye-catching NLO material. This DFT study evokes the interest of researchers regarding the development of benzimidazole-based tempting NLO compounds that could be beneficial in modern hi-tech applications.

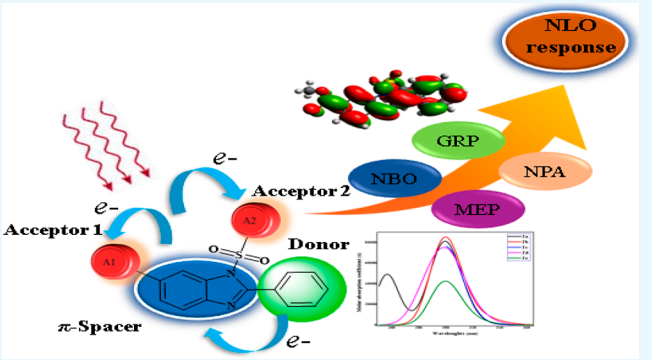

INTRODUCTION

Benzimidazoles are heterocyclic compounds also known as 1,3-benzodiazoles.[1] This bicyclic system consists of the fusion of imidazole and benzene. Benzimidazole is also a part of naturally occurring vitamin B_{12} as *N*-ribosyl-dimethylbenzimidazole.[2] In benzimidazoles, the −NH− group shows relatively strong acidic character and acts as a site for electrophilic substitution. The benzimidazole scaffold is also beneficial for the growth of molecules, which possess many pharmaceutical or biological applications. Various commercially available drugs contain benzimidazole as part of their structure,[3] as shown in Figure 1.

A variety of biological applications accompany benzimidazole and its derivatives. Derivatives containing thio, acetamido, long chains of propyl, and thiazole-amino functionalities at the −NH group result in good antiulcer activity.[4,5] Antihelmintic,[6] antiviral, anti-HIV,[7] antifungal,[8] anticancer, cardio tonic,[9] antihypertensive, and antihistaminic[10−12] activities are also associated with benzimidazoles. In chemistry, the reactivity is of key importance because it is in confidential association with the reaction mechanism, hence allowing subsequent understanding of chemical reactions as well as improving the procedure of synthesis to develop novel materials. DFT calculation is proved to be one of the prominently utilized probes for investigating the molecular properties.[13]

Herein, taking the imidazole-based structure as a reference point, various derivatives with a basic structural core of 2-phenyl-2,3-dihydro-1*H*-benzo[*d*]imidazole are designed and synthesized by modulation of the various substituent groups. A detailed literature survey has revealed that the synthesized molecules have neither been reported nor efficiently investigated in terms of NLO response so far. Therefore, an exclusive computational investigation has been done to explore their NLO

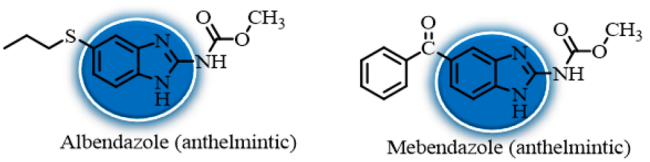

Figure 1. Commercially available drugs containing benzimidazole.

Received: May 17, 2022
Accepted: August 15, 2022
Published: August 23, 2022

Scheme 1. Reagents and Conditions: (i) MeOH, H_2SO_4, reflux 6 h; (ii) $Ni(OAc)_2$, $CHCl_3$, room temperature; (iii) $Na_2S_2O_5$, DMF, reflux 48 h; (iv) NaH, THF, 24 h stirring at room temperature

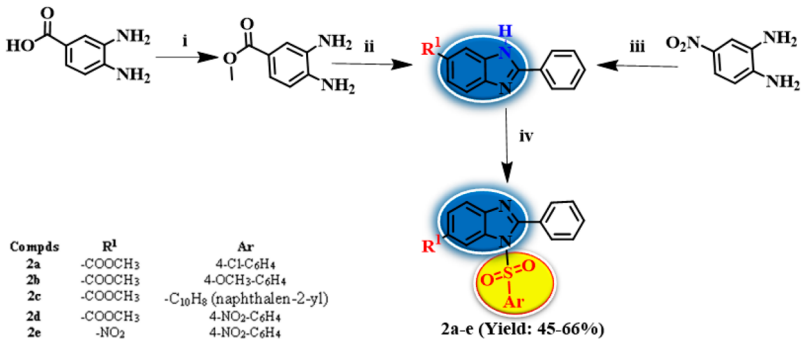

Scheme 2. Structural Modulation Representation of 2a−2e

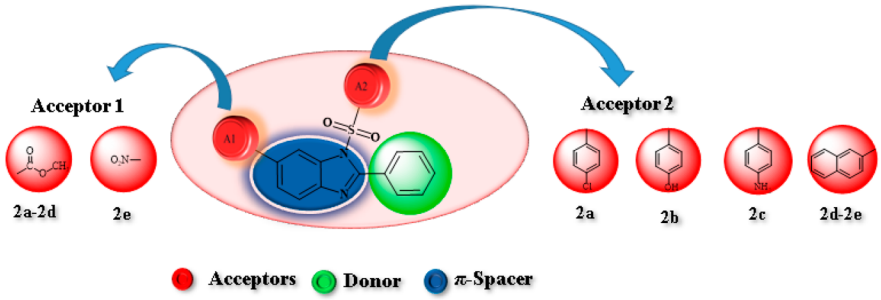

response parameters through various DFT-based analyses. So, the present DFT calculations provide a detailed account of the electronic structure, electronic transitions, molecular surfaces, global reactivity descriptors, natural population, and NLO response features of the 2-phenyl-2,3-dihydro-1*H*-benzo[*d*]-imidazole-based derivatives at the M06/6-311G(d,p) and CAM-B3LYP/6-311G(d,p) levels of theory. The optimistic opinion is that the presented DFT study will prove to be a foundation not only for the researchers but also for technicians to manufacture materials possessing extraordinary NLO behavior.

RESULTS AND DISCUSSION

Benzimidazole-based derivatives (**2a−2e**) having arylsulfonyl-moiety at the $N-1$ position were prepared in three steps as shown in Scheme 1. First of all, methyl 3,4-diaminobenzoate was synthesized from simple esterification of 3,4-diaminobenzoic acid. In the second step, 2-substituted benzimidazoles (**1**), which act as an intermediate for the formation of compounds **2a−2e**, were synthesized via two synthetic routes. In first synthetic route, methyl 3,4-diaminobenzoate was treated with benzaldehyde in the presence of nickel acetate [$Ni(OAc)_2$] using chloroform ($CHCl_3$) as a solvent. In the second synthetic route, 6-nitro-3,4-diaminobenzene was refluxed (48 h) with benzaldehyde in the presence of sodium meta-bisulphite ($Na_2S_2O_5$) using dimethylformamide (DMF) solvent to get respective intermediate **1**. In the third step, targeted *N*-sulfonyl derivatives of **1**were obtained by simple stirring (24 h) of intermediate **1** with respective arylsulfonyl chloride in the presence of sodium hydride (NaH) using tetrahydrofuran (THF) as a solvent. The compounds (**2a−2e**), which appeared as a single spot on the thin layer chromatographic (TLC) plate, separated from aqueous media via a solvent extraction technique. The characterization of compounds (**2a−2e**) was performed by well-recognized spectroscopic techniques like, FT-IR, UV, and ^1H and ^{13}C NMR.

The total numbers of proton and carbon signals are verified by ^1H and ^{13}C NMR data. In ^1H NMR, a simulated three-proton singlet is observed within the range of 3.32−3.39 ppm at CAM-B3LYP and 3.12−3.21 ppm at the M06 level of theory, which is in good correlation with experimental values (3.67−3.84 ppm) assigned to methyl ($-CH_3$) of the ester functionality. All other proton signals are seen within the aromatic region with respect to their specific integration and coupling constant values (see Tables S1−S5 and Figures S3, S7, S11, S15, and S19). In ^{13}C NMR, carbonyl carbon (C═O) is identified within the range of 165.5−167.1 ppm, which exhibited good harmony with simulated values at 163.99−164.39 ppm at CAM-B3LYP and 170.14−171.48 ppm at the M06 functional. The rest of the carbon signals are observed within the aromatic region according to the substitution pattern (see Tables S1−S5 and Figures S4, S8, S12, S16, and S20). Both ^1H and ^{13}C NMR confirmed the number of proton and carbon signals for compounds **2a−2e** (see Scheme 2).

FRONTIER MOLECULAR ORBITAL (FMO) INVESTIGATION

The FMOs investigations are regarded as significant factors in elucidating diverse perceptions like optical properties, chromophore interactions, charge transfer, chemical stability, and reactivity.[14,15] The electron-rich highest occupied molecular orbital (HOMO) possesses charge donating aptitude, while the electron-deficient lowest unoccupied molecular orbital (LUMO) manifested electron accepting capability.[16−20] Compounds with s higher E_{gap} are considered as rigid and slightly reactive and hold excellent kinetic stability. Due to this reason, the softer compounds owning smaller E_{gap} and enhanced polarizability are believed to be magnificent candidates for

https://doi.org/10.1021/acsomega.2c02805
ACS Omega 2022, 7, 31036−31046

Table 1. Computed E_{LUMO}, E_{HOMO}, and ΔE of 2a−2e

compounds	E_{HOMO}[a]	E_{LUMO}[a]	energy gaps[a]	E_{HOMO}[b]	E_{LUMO}[b]	energy gaps[b]
2a	−7.977	−0.866	7.111	−6.952	−1.960	4.992
2b	−7.815	−0.623	7.192	−6.798	−1.684	5.114
2c	−7.847	−1.076	6.771	−6.831	−2.151	4.680
2d	−8.129	−2.063	6.066	−8.129	−2.063	6.066
2e	−6.302	−2.421	3.881	−5.385	−3.543	1.842

[a]CAM-B3LYP/6-311G(d,p) level of theory, energy in eV. [b]M06/6-311G(d,p) level of theory, energy in eV.

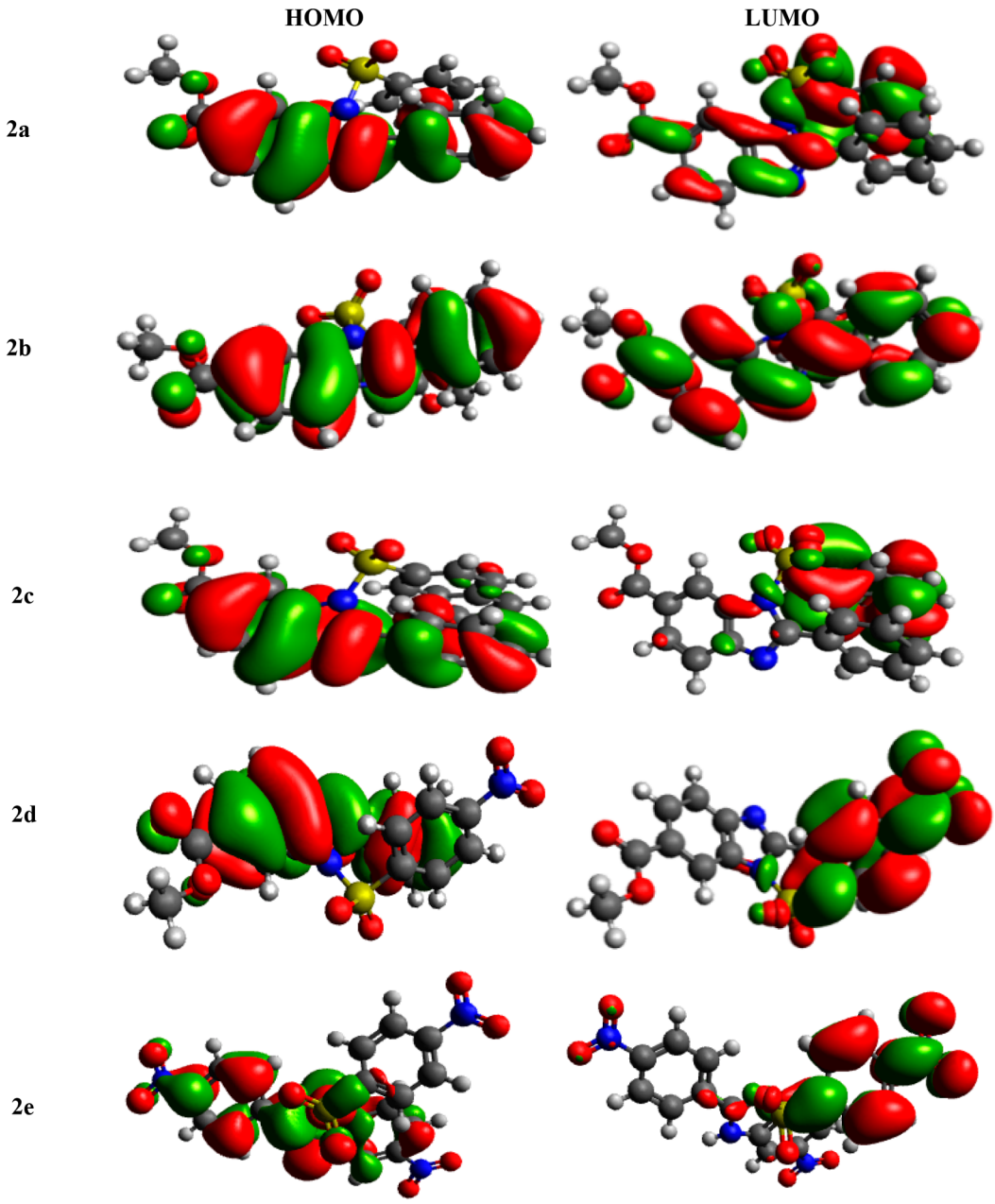

Figure 2. FMO diagrams of **2a−2e** with the CAM-B3LYP/6-311G(d,p) functional.

qualitative estimation of the NLO response.[21] The energies, i.e., E_{HOMO}, E_{LUMO}, and E_{gap}, of **2a−2e** were determined with the CAM-B3LYP/6-311G(d,p) and M06/6-311G(d,p) functionals, and their results are listed in Table 1.

Table 1 shows that the lowest energy gap is observed in **2e**, i.e., 3.881 eV with the CAM-B3LYP and 1.842 eV with the M06 functional, among all of the entitled compounds. Such a reduced energy gap is surely the consequence of increased resonance due to the introduction of strong $-NO_2$ groups at the acceptor site, which also possesses a potential $-I$ effect. Contrarily, the energy gaps calculated for **2b** and **2d** with the CAM-B3LYP and M06 functionals are 7.192 eV and 6.066 eV, respectively, which is

https://doi.org/10.1021/acsomega.2c02805
ACS Omega 2022, 7, 31036−31046

found to be the highest among all of the investigated compounds. This might be due to the existence of a hydroxyl (−OH) moiety, which has the lowest value of the −*I* effect as compared to −Cl, $-NH_2$, and $-NO_2$ groups, because of which the attraction of the electronic cloud toward the acceptor is lower. The ascending order of E_{gap} for entitled compounds at CAM-B3LYP and M06 levels of density functional theory is found to be **2e** < **2d** < **2c** < **2a** < **2b** and **2e** < **2c** < **2a** < **2b** < **2d**, respectively. Figure 2 displays the diagrammatic representation of FMOs of **2a**−**2e** compounds at CAM-B3LYP/6-311G(d,p), while FMO diagrams at the M06/6-311G(d,p) level are presented in Figure S21. From Figure 2, it can be noted that the electronic cloud is located all over the molecules in both HOMO and LUMO orbitals for **2a** and **2b** molecules, while for **2c**−**2e**, the charge density is concentrated over the whole molecule in HOMO and at A_1 in the case of LUMO (see Figures 2 and S21). With the M06 functional, the electronic cloud for LUMO/HOMO is located at the central donor and π-bridge to major and minor extents on acceptors in **2a** and **2e**. Moreover, in **2b**−**2d**, for both the LUMO and HOMO, electronic charge density is concentrated all over the molecule, except A1. An effective charge transfer from the HOMO to LUMO along with lower energy is seen for all compounds, which indicated that these compounds might prove to be the best nonlinear candidates for various NLO applications.

GLOBAL REACTIVITY PARAMETERS (GRPS)

The energies of LUMO, HOMO, and Δ*E* obtained from FMO analysis are effectively practiced to estimate global reactivity parameters (GRPs). This leads to an interpretation of internal charge transfer, stability, and chemical reactivity of **2a**−**2e**.[22−24] The compounds exhibiting a larger energy gap are considered as harder, thermodynamically stable, and lest reactive.[25] In contrast to this, compounds having smaller energy gap are regarded to be soft exhibiting a flexible nature, lesser kinetic stability, and higher reactivity.[26−28] The ionization potential alludes to the electron donating capability of a compound, while electronegativity expresses its capability to accept electrons. Chromophores with a greater value of hardness and chemical potential are regarded as stable molecules.[29] Global reactivity parameters (GRPs) for entitled chromophores are calculated by utilizing eqs S1−S7, and the results are shown in Table S36.

In this study, it is investigated that at the CAM-B3LYP level, compound **2e** has the smallest energy gap, hence it is softer and more reactive with a softness value of 0.258 eV among all the derivatives. The diminishing order of softness values is **2e** > **2d** > **2c** > **2a** > **2b**. A larger Δ*E* is demonstrated by compound **2b**, so it is less reactive with a softness value of 0.139 eV and is more stable with a greater value of hardness of 3.596 eV. The declining order of hardness values is **2b** > **2a** > **2c** > **2d** > **2e**. The greatest ionization potential value of 8.129 eV is exhibited by **2d** with an overall decreasing order of **2d** > **2a** > **2c** > **2b** > **2e**. The greater electrophilicity index value of 4.901 eV is shown by **2e** with the overall order of electrophilicity index as **2e** > **2d** > **2c** > **2a** > **2b**. By utilizing the M06 functional, compound **2e** exhibits the smallest energy gap, so it is more reactive and softer. The descending order of softness is **2e** > **2c** > **2a** > **2b** > **2d**. The larger energy gap is exhibited by compound **2b**; hence, it is less reactive and soft with a softness value of 0.196 eV and has a greater hardness value of 2.557 eV with more stability. The decreasing order of hardness values is as follows: **2d** > **2b** > **2a** > **2c** > **2e**. Compound **2d** exhibits a much greater value of ionization potential as 8.129 eV with a decreasing order of **2d** > **2a** > **2c** > **2b** > **2e**. A larger value of the electrophilicity index (10.818eV) is demonstrated by compound **2e** with a smaller value of hardness and greater value of softness. The overall order of electrophilicity index decreases as follows: **2e** > **2c** > **2d** > **2a** > **2b**. A comparative study discloses that softness values of all the compounds are greater than hardness, therefore all of these compounds are highly reactive with less kinetic stability. Hence, all of these compounds might be proven as better NLO candidates with advanced applications in modern research. From the aforementioned discussion, it is thoroughly observed that with both functionals, i.e., CAM-B3LYP and M06, the designed compound **2e** exhibits better results. In summary, the results obtained at the M06 level are observed to be potentially better in comparison with those for CAM-B3LYP. Therefore, M06 is the best suited level for investigating the NLO response of the afore-mentioned molecules.

NATURAL BOND ORBITAL (NBO) ANALYSIS

The NBO investigation is revealed as an adept technique to examine the interactions between various bonds and to examine the charge transfer process among filled and vacant orbitals.[30,31] The stabilization energies are calculated on account of this charge transfer process, and their higher values indicate reliable donor−acceptor interactions.[32,33] In this scenario, a better understanding of occupied and unoccupied orbitals is gained.[34] The two levels of theory were utilized, i.e., CAM-B3LYP and M06 for performing an NBO analysis on the optimized structures of compounds **2a**−**2e**. The results studied for CAM-B3LYP and M06 functionals are tabulated in Tables S6−S10 and S11−S15, respectively. The second-order perturbation method is used to obtain stabilization energies in NBO analysis through eq 1.

$$E^{(2)} = q_i \frac{(F_{i,j})^2}{\varepsilon_j - \varepsilon_i} \quad (1)$$

where *i* and *j* represent the donor and acceptor, accordingly; q_i, ε_i, ε_j, and $F_{i,j}$ represent the orbital occupancy and the diagonal and off-diagonal NBO Fock matrixes, while $E^{(2)}$ refers to the stabilization energy elements.

The CT from donor (occupied orbitals) to acceptor (unoccupied orbitals) is calculated among four kinds of electronic transitions in all of the studied compounds. These transitions include $\pi \rightarrow \pi^*$, $\sigma \rightarrow \sigma^*$, LP $\rightarrow \pi^*$, and LP $\rightarrow \sigma^*$, among which the most important type is $\pi \rightarrow \pi^*$ due to the conjugation of π electrons. The $\sigma \rightarrow \sigma^*$ transitions are less dominant, and LP $\rightarrow \sigma^*$ and LP $\rightarrow \pi^*$ are dominant electronic excitations. The CT in chromophores can be investigated by investigating the major $\pi \rightarrow \pi^*$ transitions.

The study performed with CAM-B3LYP shoed in compound **2a** that π(C32−C38) → π*(C27−C29) displayed a maximum stabilization energy of 34.76 kcal/mol while π(C22−O23) → π*(C17−C21) presented the smallest energy of 4.63 kcal/mol. Among $\sigma \rightarrow \sigma^*$ transitions, the superior energy of stabilization of 8.03 kcal/mol is observed in the σ(C17−C21) → σ*(C11−N13) transition. Likewise, σ(C22−O39) → σ*(C40−H42) presents the lowest energy value of 0.50 kcal/mol. The transition LP2(O39) → π*(C22−C23) showed a 58.88 kcal/mol energy value which displayed the greater stability. The energy value of 38.51 kcal/mol is observed as the lowest energy value due to the LP2(O23) → σ*(C22−O39) transition.

In compound **2b**, the π(C32−C34) → π*(C27−C29) transition with a 42.83 kcal/mol energy value has a greater

https://doi.org/10.1021/acsomega.2c02805
ACS Omega 2022, 7, 31036−31046

value of stabilization. In addition, the transition from π(C22−O23) → π^*(C17−C21), with 4.60 kcal/mol, expressed a lower value. The largest $\sigma \rightarrow \sigma^*$ transition energy value of 7.96 kcal/mol is shown by σ(C17−C21) → σ^*(C11−N13) in **2b**, and the lowest value is 0.51 kcal/mol in σ(C22−O44) → σ^*(C45−H47). Among electronic transitions, the largest feasible transition is LP2(O44) → π^*(C22−O23), and the lowest transition is LP2(O23) → σ^*(C22−O44), observed to have 58.68 and 38.54 kcal/mol stabilization energy values, respectively.

In the case of **2c**, the highest and the lowest $\pi \rightarrow \pi^*$ transitions are π(C5−C36) → π^*(C3−C4) and π(C3−C4) → π^*(C27−C28) with stabilization energy values of 33.06 kcal/mol and 0.51 kcal/mol, respectively. Additionally, in $\sigma \rightarrow \sigma^*$ transitions, 7.99 kcal/mol is seen as the uppermost energy in σ(C17−C21) → σ^*(C11−N13), and σ(S24−O25) → σ^*(C27−C29) displayed the slightest energy of 0.51 kcal/mol. Among the transitions including the lone pair (LP), the highest value of energy, i.e., 58.76 kcal/mol, is observed for transition LP2(O38) → π^*(C22−O23), while the transition LP2(O23)→ σ^*(C22−O38) articulated the lowest energy value, i.e., 38.52 kcal/mol.

Compound **2d** exhibited a π(C5−C36) → π^*(C3−C4) transition with the uppermost energy value as 33.51 kcal/mol and π(N39−O40) → π^*(C32−C38) with the smallest stability value, i.e., 4.44 kcal/mol. The highest stabilization energy value among $\sigma \rightarrow \sigma^*$ transitions for **2d** is 8.09 kcal/mol observed in σ(C17−C21) → σ^*(C11−N13), whereas the transition σ-(C32−C38) → σ^*(C38−N39) displayed the lowest energy value of 0.50 kcal/mol. The transition LP2(O42) → π^*(C22−O23) is observed with a maximum energy of 59.04 kcal/mol and LP2(O23) → σ^*(C22−O42) with a minimum value of38.50 kcal/mol.

The chromophore **2e** showed the transition π(C1−C2) → π^*(C3−C11) with a maximum stability value of 20.36 kcal/mol. The other $\pi \rightarrow \pi^*$ transition, π(N26−O27) → π^*(C20−C22), is observed with the lowest value, i.e., 1.79 kcal/mol. The $\sigma \rightarrow \sigma^*$ transitions arise because the weaker transitions among σ (donor) and σ^* (acceptor) showed 3.49 kcal/mol as the maximum stability value in **2e** occurring during σ(C16−C20) → σ^*(C15−N29). The lowest value for the same transitions is 0.25 kcal/mol, observed in σ(S30−O32) → σ^*(S30−C33). Some prominent LP transitions include LP1(N13) → π^*(C12−C18) and LP2(O27) → σ^*(N26−O28) with 21.74 and 11.31 kcal/mol energy values, respectively.

The study performed with M06 displayed that, in compound **2a**, π(C32−C38) → π^*(C27−C29) displayed the maximum while π(C22−O23) → π^*(C17−C21) presented the minimum stabilization energy values, i.e., 24.78 and 4.05 kcal/mol, respectively. The maximum stabilization energy among $\sigma \rightarrow \sigma^*$ transitions perceived in**2a** is 7.61 kcal/mol by σ(C17−C21) → σ^*(C11−N13). Likewise, σ(C28−H31) → σ^*(S24−C27) presented the lowest stabilization energy value of 0.51 kcal/mol. The transitions like LP2(O39) → π^*(C22−O23) and LP2-(O23) → σ^*(C22−O39) are observed with maximal and minimal stability values of 48.46 and 34.65 kcal/mol, respectively.

In **2b**, the π(C32−C34) → π^*(C27−C29) transition showed the greatest value of stabilization energy, i.e., 30.73 kcal/mol. In addition, transitions like π(C22−O23) → π^*(C17−C21) expressed the lowest value of 4.02 kcal/mol. Furthermore, the energy value of 7.55 kcal/mol is observed in σ(C17−C21) → σ^*(C11−N13) as the largest value among $\sigma \rightarrow \sigma^*$ transitions. The other electronic interaction, σ(S24−O25) → σ^*(C27−C29), expressed the minimal stability as 0.53 kcal/mol. Among other transitions, the uppermost probable transition is LP2-(O44) → π^*(C22−O23) with a 48.30 kcal/mol energy value, and LP2(O23) → σ^*(C22−O44) showed the lowest energy of 34.69 kcal/mol.

In **2c**, the π(C5−C36) → π^*(C3−C4) transition exhibited 23.70 kcal/mol and π(C3−C4) → π^*(C29−C32) exhibited 0.54 kcal/mol, regarded as the highest and the lowest stabilization energies, respectively. Among $\sigma \rightarrow \sigma^*$ transitions, 7.58 kcal/mol is noted as the largest stability value in σ(C17−C21) → σ^*(C11−N13), and σ(S24−C27) → σ^*(C28−H31) exhibited the lowest energy value of 0.52 kcal/mol. The highest stability (48.36 kcal/mol) is noted for transition LP2(O38) → π^*(C22−O23) due to resonance. The transition LP2(O23) → σ^*(C22−O38) expressed the lowest stability value of 34.66 kcal/mol.

The most important $\pi \rightarrow \pi^*$ transitions in compound **2d** are π(C32−C38) → π^*(N39−O40) and π(N39−O40) → π^*(C32−C38) and exhibited the highest and the lowest stabilization energy values, i.e., 24.42 and 4.01 kcal/mol, respectively. Amidst the weaker $\sigma \rightarrow \sigma^*$ excitations, 7.67 kcal/mol is perceived as the greater value of energy shown in σ(C17−C21) → σ^*(C11−N13), while σ(C15−H16) → σ^*(N12−C14) displayed the lowest energy value of 0.50 kcal/mol. The excitation LP2(O42) → π^*(C22−O23) is observed with a maximum energy of 48.59 kcal/mol, and LP2(O23) → σ^*(C22−O42) showed the minimum value of 34.64 kcal/mol.

In the case of **2e**, the transition with the utmost energy value is π(C1−C2) → π^*(C3−C11), exhibiting 15.24 kcal/mol, while π(N26−O27) → π^*(C20−C22) is the lowest energy transition of the same type, i.e., 1.60 kcal/mol. The energy value of 3.30 kcal/mol arising by much weaker interactions is perceived as a greater value in **2e** for the σ(C16−C20) → σ^*(C15−N29) transition, while the transition from σ(C20−C22) → σ^*(C22−N26) showed the smallest energy value of 0.25 kcal/mol. The electronic transition LP1 (N13) → π^*(C12−C18) is noted as the highest stability excitation with 18.19 kcal/mol, and LP2(O27)→ σ^*(N26−O28) with 10.33 kcal/mol exhibited the lowest value.

Overall data revealed that the delocalization of π-electrons plays a remarkable role in the stability of molecules. Therefore, we can assume the prolonged hyperconjugation is present in entitled compounds and plays a major role in their stabilization and provides an excellent NLO response.

VIBRATIONAL ANALYSIS

DFT investigations were conducted in order to understand the vibration bands associated with **2a**−**2e** in the gas phase. The complete data at two levels of theory, i.e., CAM-B3LYP/6-311G(d,p) and M06/6-311G(d,p), were computed to examine the absorption bands and intensities related with specific vibrations, and the results are given in Tables S16−S25, while their experimental spectra are found in Figures S2, S6, S10, S14, and S18.

C−H Stretching Vibration. In **2a** at the CAM-B3LYP level, the computed carbon−hydrogen (C−H) stretching modes occurred at 3281−3073 cm^{-1}, which is in good harmony with the experimentally determined value, i.e., 3050 cm^{-1}. The C−H stretching bands of the aromatic ring are shown as mixed symmetrical and antisymmetric modes at 3223−3183 cm^{-1}. The C−H stretching modes and other modes and their intensities are additionally determined at the lowest frequencies, as shown in Table S16. The rocking vibration modes are noted to be 1544−

https://doi.org/10.1021/acsomega.2c02805
ACS Omega 2022, 7, 31036−31046

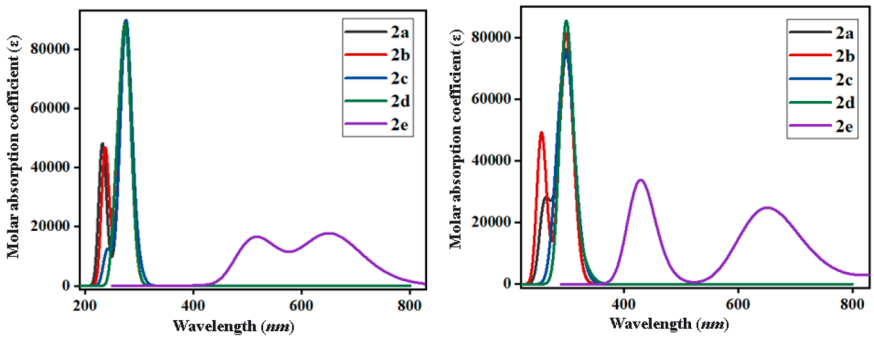

Figure 3. Absorption spectra of **2a**−**2e** at CAM-B3LYP (left) and M06 (right) levels of theory in combination with the 6-311G (d,p) basis set.

1037 cm^{-1} with experimental values at 1300−980 cm^{-1} and wagging at 805 cm^{-1}, as displayed in Table S16. Similarly, in **2a** at M06, the carbon−hydrogen (C−H) stretching vibrational mode is found at 3228−3024 cm^{-1}. However, the frequency mode at 3177−3024 cm^{-1} is observed as mixed asymmetric and symmetric stretching of C−H. The computed rocking vibrations found in the range of 1595−1009 cm^{-1} while wagging at 863−838 cm^{-1} is shown in Table S21. The afore-mentioned frequencies show harmony with the experimental values (see Figure S2). For **2b** at CAM-B3LYP, the C−H stretching frequencies are located in the range of 3282−3038 cm^{-1}, as shown in Table S17. The aromatic ring C−H stretching bands are displayed as symmetric and asymmetric modes at 3211−3104 cm^{-1}. However, 3104−3038 cm^{-1} is displayed for symmetric and asymmetric stretching of the C−H bond in the methyl group. The rocking and wagging frequencies are obtained at 1555−1042 cm^{-1}, showing harmony with the experimental value (1570 cm^{-1}). At M06, the carbon−hydrogen (C−H) stretching vibrational mode is noted at 3235−3002 cm^{-1}. The frequency mode in the range of 3191−3119 cm^{-1} is observed as mixed asymmetric and symmetric stretching of C−H, as shown in Table S22. The computed rocking and wagging vibrational frequencies are found at 1590−1015 cm^{-1}, and the experimentally determined frequency band is seen at 1570 cm^{-1}, as given in Table S22. In **2c** at CAM-B3LYP, the C−H stretching frequencies appear at 3275−3072 cm^{-1}, as shown in Table S18. In the aromatic ring, C−H stretching is shown in the symmetric and asymmetric modes of C−H at 3212−3146 cm^{-1}. The rocking and wagging frequencies are archived in the range of 1543−1039 cm^{-1} and expressed a good relationship when compared with the experimental value (1310 cm^{-1}). Similarly, at M06, the carbon−hydrogen stretching vibrational mode at 3231−3024 cm^{-1} and the vibrational band at 3177−3105 cm^{-1} are observed as mixed symmetric and asymmetric stretching of C−H, as shown in Table S23. The C−H rocking frequency range is found at 1513−1092 cm^{-1}, while its experimental value was 1310 cm^{-1} and wagging vibrational value was 861 cm^{-1}, given in Table S23. Similarly, in **2d** and **2e** at CAM-B3LYP, the C−H stretching modes are examined at 3280−3074 and 3255−3199 cm^{-1}, respectively, as shown in Tables S19 and S20. In the aromatic ring, the afore-mentioned vibrational modes for symmetric and asymmetric modes exist in the ranges of 3213−3148 and 3249−3199 cm^{-1}, respectively. These vibrational frequencies are in excellent correlation with their experimentally determined vibrational modes (see Figures S19 and S20). The other C−H stretching bands are also collected at low frequencies, as shown in Tables S19 and S20. The rocking frequencies are found to be at 1544−1039 and 1576−1058 cm^{-1}, respectively, for **2d** and **2e**. The experimental values for the above-mentioned frequencies are examined at 1200 and 922 cm^{-1} as shown in Tables S19 and S20. At M06, the carbon−hydrogen stretching vibrational mode is noted in the range of 3234−3025 cm^{-1}. In the same manner, the mixed symmetric and asymmetric frequencies of the C−H mode are computed in the ranges of 3203−3108 and 3203−3156 cm^{-1}, accordingly (Tables S24 and S25). The rocking and wagging frequencies are found at 1512−1090 and 837 cm^{-1}, respectively.

C−C Stretching Vibrations. At CAM-B3LYP, the C−C stretching bands appeared in the range of 1685−1530 cm^{-1} in **2a**, 1676−1512 cm^{-1} in **2b**, 1685−1532 cm^{-1} in **2c**, 1715−1508 cm^{-1} in **2d**, and 1714−1520 cm^{-1} in **2e**, which showed good agreement with the experimental values as represented in Figures S2, S6, S10, S14, and S18, respectively. Nevertheless, at M06, the C−C stretching vibrations observed at 1660−1512 cm^{-1} in **2a**, 1655−1528 cm^{-1} in **2b**, 1661−1513 cm^{-1} in **2c**, 1718−1507 cm^{-1} in **2d**, and 1711−1555 cm^{-1} in **2e** are shown in Tables S21−S25.

C−N Bands. In **2a** at CAM-B3LYP, the C−N stretching bands are seen at 1615, 1347, and 1248 cm^{-1}. The afore-mentioned vibrational modes are observed at 1611, 1349, and 1249 in **2b**. Likewise, the C−N mode of **2c** appeared at 1611, 1382, and 1247 cm^{-1} (Tables S16−S18). These modes are observed at 1617, 1447, and 1247 cm^{-1} in **2d**, shown in Table S19. Similarly, modes are observed at 1640, 1308, and 1213 cm^{-1} in **2d**, shown in Table S20. However, in **2a** at M06, the C−N stretching vibrations observed at 1631, 1318, and 1255 cm^{-1} in **2b**; 1593, 1332, and 1296 cm^{-1} in **2c**; 1598, 1366, and 1257 cm^{-1} in **2d**; and 1626, 1311, and 1241 cm^{-1} in **2e** are shown in Tables S21−S25. Good harmony is seen when compared with experimental absorption bands (see Figures S2, S6, S10, S14 and S18).

C−O Bands. In **2a** at CAM-B3LYP, the C−O stretching modes are observed at 1827, 1381, and 1248 cm^{-1} (Table S16). Moreover, the C−O stretching bands are noted at 1826, 1349, and 1249 cm^{-1} in **2b** (Table S17). Furthermore, in **2c** the C−O stretching modes are seen at 1827, 1711, 1382, and 1247 cm^{-1} (Table S18). The C−O stretching modes are examined at 1829, 1345, and 1247 cm^{-1} in **2d** (Table S19), and in **2e** these vibrational bands are found at 1717, 1347, and 1213 cm^{-1} (Table S20). Similarly, at M06, the C−C stretching vibrations observed at 1837, 1392, and 1255 cm^{-1} in **2a**; at 1832, 1328, and 1271 cm^{-1} in **2b**; at 1835, 1332, and 1232 cm^{-1} in **2c**; at 1838, 1330, and 1230 cm^{-1} in **2d**; and 1721, 1398, and 1241 cm^{-1} in **2e** are shown in Tables S21−S25. At both levels of theory, the experimental values showed good agreement with the

https://doi.org/10.1021/acsomega.2c02805
ACS Omega 2022, 7, 31036−31046

Table 2. Computed Dipole Moment, Linear Polarizability, and Hyperpolarizability of 2a−2e

properties	2a	2b	2c	2d	2e
μ_{total} [a]	4.15	7.49	6.24	2.33	3.04
$\langle\alpha\rangle$ [a]	3.168×10^{-23}	4.198×10^{-23}	4.614×10^{-23}	4.142×10^{-23}	4.866×10^{-23}
β_{total} [a]	6.037×10^{-30}	5.782×10^{-30}	5.029×10^{-30}	5.537×10^{-30}	5.095×10^{-29}
μ_{total} [b]	4.34	7.52	6.27	2.39	3.0406
$\langle\alpha\rangle$ [b]	3.220×10^{-23}	4.331×10^{-23}	4.760×10^{-23}	4.287×10^{-23}	5.379×10^{-23}
β_{total} [b]	5.812×10^{-30}	5.637×10^{-30}	5.577×10^{-30}	9.230×10^{-30}	2.0418×10^{-28}

[a]CAM-B3LYP. [b]M06, dipole moment in Debye while $\langle\alpha\rangle$ and β_{total} are in esu.

theoretical values as represented in Figures S2, S6, S10, S14, and S18, respectively.

OPTICAL ANALYSIS

UV−visible spectroscopy provides aid in understanding the types of transitions, leading to the arrangement of transitions and the potential of transport of charge in compounds.[35,36] The excitations in absorption spectra of **2a−2e** (Figure 3) were estimated by using TD-DFT analysis at two different levels of theory, i.e., CAM-B3LYP and M06. Six lower singlet−singlet transitions were examined utilizing TD-DFT analysis, and the absorbance spectra of **2a−2e** are included in Figures S1, S5, S9, S13, and S17. Tables S26−S30 and S31−S35 present the computed transition energies (E_{ge}), absorbance wavelengths (λ_{max}), oscillation strength (f_{os}), and transition type for each compound under investigation at CAM-B3LYP and M06, respectively.

The values of maximum absorbance for **2a−2e** are found to be 275.355, 275.160, 290.927, 278.347, and 652.858 nm, accordingly, with the CAM-B3LYP functional. Similarly, the λ_{max} values calculated at the M06 level of theory are noted to be 300.260, 299.522, 317.095, 299.464, and 428.611 nm, respectively. Their experimental absorbance spectra showed the maximum absorbance nearly at 305, 275, 309, 280, and 345 nm for **2a−2e**, respectively. These calculations disclosed that experimental results showed good harmony with the M06 functional and indicated it to be a suitable level for further investigation of these compounds. Therefore, by comparing the results at the M06 level, the highest absorption value is observed in **2e** with the lowest transition energy value of 2.893 eV, which demonstrated it to be the most red-shifted compound among all entitled chromophores, while **2b** and **2d** are examined as the blue-shifted compounds with higher excitation energies of 4.139 and 4.140 eV, accordingly. Overall, the descending order of absorption values of molecules is **2e** > **2c** > **2a** > **2b** > **2d**. Compound **2e** with a lower excitation energy and greater λ_{max} might show an appealing NLO response.

NONLINEAR OPTICAL (NLO) ANALYSIS

In the modern era, many fields like signal processing, optical switches, telecommunication technologies, and optical storage systems require intensive utilization of NLO substances.[37] The objective of NLO is to explain the response of molecules to an applied electric field. The optical response is governed via electrical properties of the compound that are associated with nonlinear (hyperpolarizability, β) and linear (polarizability, $\langle\alpha\rangle$) interactions. Nevertheless, determining the NLO properties of large delocalized π-systems utilizing the DFT approach is a substantial challenge. Nonlinearity in organic molecules is deeply linked to the functional property relationship, which can be modified synthetically by estimating the effect of different donor−acceptor molecules and modifying the structure of π-conjugated systems.[38] Charge transport efficiency is consistently higher in substances with substantial NLO characteristics.[39,40] The NLO response of the **2a−2e** series of compounds was computed at two functionals [CAM-B3LYP/6-311G(d,p) and M06/6-311G(d,p)], and their results are presented in the Tables 2 and S37−S40, respectively.

The dipole polarizability $\langle\alpha\rangle$ explains the capacity of a compound to create an induced dipole moment when placed in an external electric field. Understanding this fundamental response attribute is crucial for explaining nonbonded interactions such as induction and dispersion among the molecules in condensed or cluster phases. Additionally, understanding the dipole polarizability is crucial for designing organic electro-optic (OPE) and NLO materials.[41] Moreover, the contributions of tensors are quite significant as they allow the formation of well-separated spin-depended traps and a mutual orientation of atomic polarization and light polarization. In our studied compounds, the significant contribution tensor is found to be α_{xx} (see Tables S37 and S39). At CAMB3LYP, the $\langle\alpha\rangle$ values of **2a−2e** compounds are as follows: 168, 4.198, 4.614, 4.142, and 4.866×10^{-23} esu. At the M06 level, the values are 3.220, 4.331, 4.760, 4.287, and 5.379×10^{-23} esu, respectively. The linear polarizability response is found to be almost the same for both functionals, and the decreasing order is noted as **2e** > **2c** > **2b** > **2d** > **2a**. The dipole moment values are 4.15, 7.49, 6.24, 2.33, and 3.04 D for **2a−2e**, respectively. The largest value of the dipole moment, i.e., 7.49 D, is shown by compound **2b**, while **2d** showed the smallest value, i.e., 2.33 D. The overall descending order for the values of the dipole moment is **2b** > **2c** > **2a** > **2e** > **2d**. The values of hyperpolarizability (β_{tot}) and its nine contributing tensors along x, y, and z directions are expressed in Tables S38 and S40. A literature survey has revealed that the ΔE between the LUMO and HOMO affected the polarizability of the compounds. Generally, the molecules with a lower energy gap show large hyperpolarizability values.[42,43] In our synthesized compounds, **2e** exhibited the highest hyperpolarizability response, i.e., 5.095×10^{-29} and 2.0418×10^{-28} esu, while **2c** exhibited the lowest values of hyperpolarizability, *i.e.*, 5.029×10^{-30} and 5.577×10^{-30} esu with the CAM-B3LYP and M06 functionals, respectively. All investigated compounds follow the given decreasing order of hyperpolarizability: **2e** > **2a** > **2b** > **2d** > **2c** at CAM-B3LYP with a slightly different order at M06, i.e., **2e** > **2d** > **2a** > **2b** > **2c**. By comparing the results at both levels, M06 showed comparatively better results than CAM-B3LYP. A comparative analysis was also performed by utilizing the urea molecule, which is utilized as a standard compound (μ = 3.4 D, $\langle\alpha\rangle = 4.878 \times 10^{-23}$ esu, and $\beta_{total} = 0.3728 \times 10^{-30}$ esu). By making a comparison of the dipole moments between urea and **2a−2e** compounds—1.29, 2.20, 1.83, 0.68, and 0.89 at CAM-B3LYP and 1.27, 2.21, 1.84, 0.7, and 0.89 at M06—the aforementioned compounds show greater μ values than those of urea. For dipole polarizability, the above-mentioned compounds

https://doi.org/10.1021/acsomega.2c02805
ACS Omega 2022, 7, 31036−31046

showed a comparable response, while for first-order hyperpolarizability, the expressed 16.1, 16.5, 13.4, 15 and 137 at CAM-B3LYP and 15.5, 15.1, 14.9, 24.7, and 54.77 with the M06 functional show a greater NLO response than that of urea molecule. Interestingly, a more appealing NLO response is studied for prepared compounds than that for the urea molecule, which indicated their significance as used in photonic material.

Natural bond orbital (NBO) charges can help to explain the phenomenon of electronegativity balancing, kinetics of atomic charge mechanisms, and electrostatic potential on the external surface of structures.[44] The structure and bonding efficiency of molecules are significantly influenced by atomic electrical charges.[45] The electronic density distribution over the aromatic ring is uneven in the existence of sufficient electronegative elements like O and N in the designed compounds, in accordance with Mulliken population data.[46] The objective of utilizing a quantum chemical methodology is to accurately explain the electron distributions throughout the different chromophores and to predict the reactivity of the represented charges.[47] As shown by Figure S22, Mulliken atomic charges of **2a**−**2e** are computed via CAM-B3LYP/6-311G(d,p) and M06/6-311G(d,p) approaches with the basis set, and the data are presented in Figure S22. Mulliken population analysis suggests that there is no variation in charge distribution throughout all hydrogen atoms. The sulfur atoms of SO_2, nitrogen atoms of NO_2, and some carbon of the benzene ring possess high positive charges because of the resonance effect. Whereas oxygen atoms are possessed by $-COOCH_3$ and $-OCH_3$, the nitrogen of the imidazole ring and carbon atoms of benzene rings holding $-COOCH_3$ and $-OCH_3$ groups possess high negative charges due to their highly electronegative nature.

CONCLUSION

In this study, novel *N*-1-sulfonyl substituted derivatives (**2a**−**2e**) with the D−π−A framework are synthesized, and their NLO behavior is explored. The efficient electron withdrawing acceptors are utilized for their structural tailoring, which strengthened the charge transfer phenomena. Different spectroscopic techniques, UV−visible, FTIR, and ^{1}H and ^{13}C NMR, are utilized for the determination of structural characterization. Besides the synthesis, a computational study was also performed in order to explore the NLO characteristics of **2a**−**2e**. FMO analysis explained the effective intramolecular charge transfer (ICT) of molecules. The NBO results depicted the development of a charge separation state owing to the effective transference of electrons in the π-conjugated schemes of **2a**−**2e**. The UV−visible analysis proved compound **2e** to be the most red-shifted among all other synthesized compounds, having a reduced energy gap. Further, global reactivity parameters (GRPs) findings support the FMO and UV−vis investigations as a higher value of softness is seen for this molecule, elucidating it as a more reactive compound. Therefore, the efficient linear and nonlinear response ($\langle\alpha\rangle$ = 4.866 × 10^{-23} and 5.379 × 10^{-23}esu while β_{tot} = 5.095 × 10^{-29} and 2.0418 × 10^{-28} esu) is also studied for this molecule. This NLO study has illustrated the *N*-1-sulfonyl substituted derivatives as excellent materials for researchers to disclose advanced applications in optoelectronics and the telecommunication sector.

EXPERIMENTAL PROCEDURE

Substrate and Reagents. Benzaldehyde (Applichem, Germany), 3,4-diaminobenzoic acid, ethanol, *tetra*-hydrofuran (THF) 99%, sulfuric acid 98%, nickel acetate (Merck, Germany), methanol, chloroform, *n*-hexane, dichloromethane (Riedel-de-Haen, Germany) and sodium hydride, 4-nitrobenzenesulfonyl chloride 97%, 4-chlorobenzenesulfonyl chloride, 4-methoxybenzenesulfonyl chloride 97%, 2-naphthalenesulfonyl chloride 99% (Sigma-Aldrich, USA) were of high purity grade and used as received.

Instrumentation. The progress and purity of the reaction was monitored using precoated silica gel 60 F_{254} aluminum thin layer chromatographic sheets (Merck, Germany). Melting points were determined with an A&E Lab (UK) melting point apparatus and are uncorrected. To determine the characteristic functional groups in the compounds, infrared spectra were recorded on a Shimadzu Nicolet iS10 FT-IR spectrophotometer. ^{1}H and ^{13}C NMR spectra were recorded on a Bruker Avance 300 MHz spectrometer.

General Procedure for the Synthesis of *N*-1-Sulfonyl Substituted Derivatives of 2-Substituted Benzimidazoles (2a−2e). The respective 2-substituted benzimidazoles (0.2 *g*, 0.01 mmol) and sodium hydride (1.0 equiv) were dissolved in THF solvent, and the temperature of the reaction mixture was maintained between 5 and 10 °C. The reaction mixture was stirred for 30 min. Then, respective arylsulfonyl chloride (1.20 equiv) was added, and reaction mixture was left for 24 h on stirring at room temperature. The progress of the reaction was continuously monitored by taking TLC (*n*-hexane/ethyl acetate, 3:2) after every 1 h. Upon completion, the reaction mixture was poured on ground ice. The product was extracted via solvent extraction using dichloromethane solvent, and the organic layer was separated. The solvent was evaporated under a high vacuum to obtain a dried product. Finally, the purity of the synthesized compounds was ascertained by recrystallization in ethanol.

*Methyl 1-(4-Chlorophenylsulfonyl)-2-phenyl-1H-benzo-[d]imidazole-6-carboxylate (**2a**).* Light brown shiny solid. Yield: 60%. Melting point: 167−168 °C. R_f: 0.52 (*n*-hexane/ethyl acetate; 3:2). IR (ATR, cm^{-1}): 2950 (C−H aliphatic stretching),1708 (C═O stretching), 1570 (C═N stretching), 1530−1420 (C═C aromatic ring stretching). ^{1}H NMR (300 MHz, $DMSO_{d6}$): δ 3.84 (3H, s, $-CH_3$ ester), 7.02 (2H, d, Ar−H, J = 6.7 Hz), 7.20 (3H, m, Ar−H), 7.56 (2H, m, Ar−H), 7.75 (2H, d, Ar−H, J = 7.8 Hz), 7.84 (1H, d, Ar−H, J = 8.4 Hz), 7.92 (1H, dd, Ar−H, J = 8.4, 1.5 Hz), 8.11 (1H, s, Ar−H). ^{13}C NMR (75 MHz, $DMSO_{d6}$): 52.6 ($-CH_3$ ester), 113.5, 119.6, 124.0, 124.5, 126.4, 127.9, 128.1, 129.4, 129.6, 129.7, 130.9, 136.0, 137.0, 146.2, 156.6 (Ar−C), 166.9 (C═O).

*Methyl 1-(4-Methoxyphenylsulfonyl)-2-phenyl-1H-benzo-[d]imidazole-6-carboxylate (**2b**).* Light brown solids. Yield: 66%. Melting point: 173−174 °C. R_f: 0.50 (*n*-hexane/ethyl acetate, 3:2). IR(ATR, cm^{-1}): 2943 (C−H aliphatic stretching), 1705 (C═O stretching), 1562 (C═N stretching), 1516−1442 (C═C aromatic ring stretching). ^{1}H NMR (300 MHz, $DMSO_{d6}$): δ 3.84 (3H, s, $-CH_3$ ester), 6.99 (2H, d, Ar−H, J = 6.7 Hz), 7.28 (3H, m, Ar−H), 7.53 (2H, m, Ar−H), 7.75 (2H, d, Ar−H, J = 7.8 Hz), 7.84 (1H, d, Ar−H, J = 8.4Hz), 7.92 (1H, dd, Ar−H, J = 8.4, 1.5 Hz), 8.10 (1H, s, Ar−H). ^{13}C NMR (75 MHz, $DMSO_{d6}$): 52.6 ($-CH_3$ ester), 55.6 ($-OCH_3$), 113.2, 113.6, 124.2, 124.6, 126.4, 127.5, 128.1, 129.4, 129.6, 131.1, 135.9, 136.9, 145.6, 156.5 (Ar−C), 166.9 (C═O).

*Methyl 1-(Naphthalen-2-ylsulfonyl)-2-phenyl-1H-benzo-[d]imidazole-6-carboxylate (**2c**).* Black solid. Yield: 60%. Melting point: 86−87 °C. R_f: 0.48 (*n*-hexane/ethyl acetate. 3:2). IR (ATR, cm^{-1}): 2916 (C−H aliphatic stretching), 1716

https://doi.org/10.1021/acsomega.2c02805
ACS Omega 2022, 7, 31036−31046

(C═O stretching), 1581 (C═N stretching), 1543−1435 (C═C aromatic ring stretching). ^{1}H NMR (300 MHz, $DMSO_{d6}$): δ 3.80 (3H, s, $-CH_3$ ester), 7.30 (1H, m, Ar−H), 7.40 (4H, m, Ar−H), 7.50 (4H, m, Ar−H), 7.80 (2H, d, Ar−H, J = 8.7 Hz), 7.90 (1H, d, Ar−H, J = 6.9 Hz), 8.00 (1H, s, Ar−H), 8.20 (1H, s, Ar−H), 8.28 (1H, s, Ar−H). ^{13}C NMR (75 MHz, $DMSO_{d6}$): δ 52.4 ($-CH_3$ ester),113.3, 119.6, 123.8, 123.9, 124.3, 126.3, 127.2, 128.0, 129.0, 129.1, 129.3, 129.5, 129.7, 129.9, 130.5, 130.9, 133.3, 154.2 (Ar−C), 167.1 (C═O).

*Methyl 1-(4-Nitrophenylsulfonyl)-2-phenyl-1H-benzo[d]-imidazole-6-carboxylate (**2d**).* Brown solid. Yield: 45%. Melting point: 130−131 °C. R_f: 0.49 (*n*-hexane/ethyl acetate, 3:2). IR (ATR,cm^{-1}): 2930 (C−H aliphatic stretching), 1720 (C═O stretching), 1585 (C═N stretching), 1531−1442 (C═C aromatic ring stretching). ^{1}H NMR (300 MHz, $DMSO_{d6}$): δ 3.67 (3H, s, $-CH_3$ ester), 6.05 (1H, s, Ar−H), 6.84 (1H, d, Ar−H, J = 8.7 Hz), 6.94 (1H,m, Ar−H), 7.73 (1H, m, Ar−H), 8.18 (4H,m, Ar−H), 8.51 (4H, m, ArH). ^{13}C NMR (75 MHz, $DMSO_{d6}$): 52.0 ($-CH_3$ ester), 115.4, 116.5, 116.9, 125.3, 131.0, 133.2, 134.4, 143.1, 151.5, 152.8 (Ar−C), 165.5 (C═O).

*6-Nitro-2-(4-nitrophenyl)-1-(4-nitrophenylsulfonyl)-1H-benzo[d]imidazole (**2e**).* Brown solid. Yield: 45%. Melting point: 232−233 °C. R_f: 0.65 (*n*-hexane/ethyl acetate;, 1:1). IR (ATR, cm^{-1}): 3030 (C−H aliphatic stretching), 1665 (C═N stretching), 1531−1442 (C═C aromatic ring stretchings). ^{1}H NMR (300 MHz, $DMSO_{d6}$): δ 6.67 (1H, d, Ar−H, J = 8.7 Hz), 7.62 (1H, d, Ar−H, J = 9.0 Hz), 7.78 (1H, d, Ar−H, J = 9.0 Hz), 7.88 (1H, d, Ar−H, J = 8.7 Hz), 7.97 (1H, s, Ar−H), 8.04 (1H, dd, Ar−H, J = 2.4 Hz), 8.13 (1H, dd, Ar−H, J = 2.1 Hz), 8.27 (1H, d, Ar−H, J = 8.7 Hz), 8.45 (3H, m, Ar−H). ^{13}C NMR (75 MHz, $DMSO_{d6}$): δ 113.9, 116.1, 117.8, 118.9, 124.7, 125.0, 128.5, 128.9, 129.5, 135.3, 143.5, 148.8, 153.9, 162.7 (Ar−C).

Computational Study. The quantum chemical analysis for all of the synthesized compounds was conducted using the Gaussian 09[48] package program with the CAM-B3LYP/6-311G (d,p) and M06/6-311G(d,p) functionals. Avogadro,[49] the GaussView 5.0[50] package, and Chemcraft[51] were utilized for various DFT and TDDFT computations along with some graphical displays of studied compounds. These investigations included UV−vis, vibrational, and ^{1}H and ^{13}C NMR techniques and the frontier molecular orbital (FMO), natural bond orbital (NBO), global reactivity parameters (GRPs), and nonlinear optical (NLO) response of imidazole-based molecules. The stabilization energy calculations of the entitled compounds were confirmed via NBO analysis and second-order perturbation theory, respectively, with the aid of the program package NBO 3.1.[52−54] By utilizing the energies of FMOs, global reactivity parameters (GRPs)[55] were calculated. The NLO parameters, i.e., dipole moment (μ), linear polarizability $\langle\alpha\rangle$ and first order hyperpolarizability (β_{tot})[56] of the title compounds were also computed by utilizing eqs S8−S10.

■ ASSOCIATED CONTENT

Supporting Information

The Supporting Information is available free of charge at https://pubs.acs.org/doi/10.1021/acsomega.2c02805.

Spectroscopic Data: UV, FT-IR, ^{1}H and ^{13}C NMR spectra of all synthesized compounds. Computational studies: frontier molecular orbitals (FMOs) of all synthesized compounds at M06/6-311G(d,p). Natural Bond Orbital (NBO) Investigations: second order perturbation theory analysis of Fock matrix in NBO of all synthesized compounds at CAM-B3LYP/6-311G(d,p). Second order perturbation theory analysis of Fock matrix in NBO of all synthesized compounds at M06/6-311G(d,p). UV−vis Analysis: wavelength, excitation energy, and oscillator strength of all investigated synthesized compounds at CAM-B3LYP/6-311G(d,p) in ethanol. Wavelength, excitation energy, and oscillator strength of all investigated synthesized compounds at M06/6-311G-(d,p) in ethanol. Nonlinear Optics: dipole polarizability and major contributing tensor (a.u.) of all studied compounds at CAM-B3LYP/6-311G (d,p). Computed first hyperpolarizabilities (β_{tot}) and major contributing tensor (a.u.) of all studied compounds at CAM-B3LYP/6-311G(d,p). Computed first hyperpolarizabilities (β_{tot}) and major contributing tensor (a.u.) of all studied compounds at M06/6-311G(d,p) (PDF)

■ AUTHOR INFORMATION

Corresponding Authors

Tashfeen Akhtar − *Department of Chemistry, Mirpur University of Science and Technology (MUST), 10250 Mirpur, Azad Jammu and Kashmir, Pakistan*; Phone: +92 (300) 5228644; Email: tashfeenchem@must.edu.pk

Muhammad Khalid − *Institute of Chemistry and Centre for Theoretical and Computational Research, Khwaja Fareed University of Engineering and Information Technology, Rahim Yar Khan 64200, Pakistan*; orcid.org/0000-0002-1899-5689; Phone: +92 (348) 6906807; Email: khalid@iq.usp.br, muhammad.khalid@kfueit.edu.pk

Aman Ullah − *Department of Agricultural, Food and Nutritional Science, Faculty of Agricultural, Life and Environmental Sciences, University of Alberta, Edmonton, Alberta T6G 2R3, Canada*; orcid.org/0000-0003-1801-0162; Email: ullah2@ualberta.ca

Authors

Shumaila Aslam − *Department of Chemistry, Mirpur University of Science and Technology (MUST), 10250 Mirpur, Azad Jammu and Kashmir, Pakistan*

Muhammad Haroon − *Department of Chemistry, Mirpur University of Science and Technology (MUST), 10250 Mirpur, Azad Jammu and Kashmir, Pakistan; Department of Chemistry, Government Major Muhammad Afzal Khan (Shaheed), Boys Degree College Afzalpur, Mirpur (Affiliated with Mirpur University of Science and Technology (MUST)), 10250 Mirpur, Azad Jammu and Kashmir, Pakistan*

Muhammad Arshad − *Department of Chemical Engineering, College of Engineering, King Khalid University, Abha 62529, Saudi Arabia*

Zahid Shafiq − *Institute of Chemical Sciences, Bahauddin Zakariya University, Multan 60800, Pakistan*

Muhammad Imran − *Department of Chemistry, Faculty of Science, King Khalid University, Abha 61413, Saudi Arabia*

Complete contact information is available at: https://pubs.acs.org/10.1021/acsomega.2c02805

Notes

The authors declare no competing financial interest.

■ ACKNOWLEDGMENTS

M.A. expresses appreciation to the Deanship of Scientific Research at King Khalid University Saudi Arabia through the

research groups program under grant number R.G.P.2/83/43. The authors are also thankful for the cooperation and collaboration of A.A.C.B. from IQ-USP, Brazil, especially for his continuous support and providing computational lab facilities.

REFERENCES

(1) Goyal, R.; Sharma, M.; Ahuja, D.; Jain, A. Synthesis and Evaluation of Phenol Derivatives of Sulfonyl Chloride Quinoxaline. *J. Drug Delivery Ther.* **2019**, *9* (4), 774−782.

(2) Barker, H. A.; Smyth, R. D.; Weissbach, H.; Toohey, J. I.; Ladd, J. t; Volcani, B. E. Isolation and Properties of Crystalline Cobamide Coenzymes Containing Benzimidazole or 5, 6-Dimethylbenzimidazole. *J. Biol. Chem.* **1960**, *235* (2), 480−488.

(3) Bhattacharya, S.; Chaudhuri, P. Medical Implications of Benzimidazole Derivatives as Drugs Designed for Targeting DNA and DNA Associated Processes. *Curr. Med. Chem.* **2008**, *15* (18), 1762−1777.

(4) Google Scholar. https://scholar.google.com/scholar?hl=en&as_sdt=0%2C5&q=Ozkay%2C+Y.%3B+Tunali%2C+Y.%3B+H%C3%BCseyin%2C+K.%3B%2C+Ilhan%2C+I.+Antimicrobial+activity+and+a+SAR+study+of+some+novel+benzimidazole+derivatives+bearing+hydrazones+moiety.+Euro.+J.+Med.+Chem.+2010%2C+45%288%29%2C+3293-3298.&btnG= (accessed July 1, 2022).

(5) Grassi, A.; Ippen, J.; Bruno, M.; Thomas, G. BAY P 1455, a Thiazolylaminobenzimidazole Derivative with Gastroprotective Properties in the Rat. *Eur. J. Pharmacol.* **1991**, *195* (2), 251−259.

(6) Saimot, A. G.; Cremieux, A. C.; Hay, J. M.; Meulemans, A.; Giovanangeli, M. D.; Delaitre, B.; Coulaud, J. P. Albendazole as a Potential Treatment for Human Hydatidosis. *Lancet* **1983**, *322* (8351), 652−656.

(7) Chimirri, A.; Grasso, S.; Monforte, A. M.; Monforte, P.; Zappala, M. Anti-HIV Agents II. Synthesis and in Vitro Anti-HIV Activity of Novel 1H, 3H-Thiazolo [3, 4-a] Benzimidazoles. *Farm. Soc. Chim. Ital. 1989* **1991**, *46* (7−8), 925−933.

(8) Berg, D.; Büchel, K.-H.; Plempel, M.; Zywietz, A. Action Mechanisms of Cell-Division-Arresting Benzimidazoles and of Sterol Biosynthesis-Inhibiting Imidazoles, 1, 2, 4-Triazoles, and Pyrimidines. *Mycoses* **1986**, *29* (5), 221−229.

(9) Piazzesi, G.; Morano, I.; Rüegg, J. C. Effect of Sulmazole and Pimobendan on Contractility of Skinned Fibres from Frog Skeletal Muscle. *Arzneimittelforschung* **1987**, *37* (10), 1141−1143.

(10) Benavides, J.; Schoemaker, H.; Dana, C.; Claustre, Y.; Delahaye, M.; Prouteau, M.; Manoury, P.; Allen, J.; Scatton, B.; Langer, S. Z. In Vivo and in Vitro Interaction of the Novel Selective Histamine H1 Receptor Antagonist Mizolastine with H1 Receptors in the Rodent. *Arzneimittelforschung* **1995**, *45* (5), 551−558.

(11) IEMURA, R.; HORI, M.; OHTAKA, H. Syntheses of the Metabolites of 1-(2-Ethoxyethyl)-2-(Hexahydro-4-Methyl-1H-1, 4-Diazepin-1-Yl)-1H-Benzimidazole Difumarate (KG-2413) and Related Compounds. *Chem. Pharm. Bull. (Tokyo)* **1989**, *37* (4), 962−966.

(12) Niemegeers, C. J. E.; Awouters, F.; Janssen, P. A. J. The Pharmacological Profile of a Specific, Safe, Effective and Non-Sedative Anti-Allergic, Astemizole. *Agents Actions* **1986**, *18* (1), 141−144.

(13) Ziegler, T. Approximate Density Functional Theory as a Practical Tool in Molecular Energetics and Dynamics. *Chem. Rev.* **1991**, *91* (5), 651−667.

(14) Khalid, M.; Ali, A.; Khan, M. U.; Tahir, M. N.; Ahmad, A.; Ashfaq, M.; Hussain, R.; de Alcantara Morais, S. F.; Braga, A. A. C. Non-Covalent Interactions Abetted Supramolecular Arrangements of N-Substituted Benzylidene Acetohydrazide to Direct Its Solid-State Network. *J. Mol. Struct.* **2021**, *1230*, 129827.

(15) Adeel, M.; Khalid, M.; Ullah, M. A.; Muhammad, S.; Khan, M. U.; Tahir, M. N.; Khan, I.; Asghar, M.; Mughal, K. S. Exploration of CH··· F & CF··· H Mediated Supramolecular Arrangements into Fluorinated Terphenyls and Theoretical Prediction of Their Third-Order Nonlinear Optical Response. *RSC Adv.* **2021**, *11* (14), 7766−7778.

(16) Khalid, M.; Jawaria, R.; Khan, M. U.; Braga, A. A. C.; Shafiq, Z.; Imran, M.; Zafar, H. M. A.; Irfan, A. An Efficient Synthesis, Spectroscopic Characterization, and Optical Nonlinearity Response of Novel Salicylaldehyde Thiosemicarbazone Derivatives. *ACS Omega* **2021**, *6* (24), 16058−16065.

(17) Khan, M. U.; Khalid, M.; Khera, R. A.; Akhtar, M. N.; Abbas, A.; Rehman, M. F. u.; Braga, A. A. C.; Alam, M. M.; Imran, M.; Wang, Y.; Lu, C. Influence of Acceptor Tethering on the Performance of Nonlinear Optical Properties for Pyrene-Based Materials with A-π-D-π-D Architecture. *Arab. J. Chem.* **2022**, *15* (3), 103673.

(18) Adeel, M.; Braga, A. A.; Tahir, M. N.; Haq, F.; Khalid, M.; Halim, M. A. Synthesis, X-Ray Crystallographic, Spectroscopic and Computational Studies of Aminothiazole Derivatives. *J. Mol. Struct.* **2017**, *1131*, 136−148.

(19) Shahid, M.; Salim, M.; Khalid, M.; Tahir, M. N.; Khan, M. U.; Braga, A. A. C. Synthetic, XRD, Non-Covalent Interactions and Solvent Dependent Nonlinear Optical Studies of Sulfadiazine-Ortho-Vanillin Schiff Base:(E)-4-((2-Hydroxy-3-Methoxy-Benzylidene) Amino)-N-(Pyrimidin-2-Yl) Benzene-Sulfonamide. *J. Mol. Struct.* **2018**, *1161*, 66−75.

(20) Khalid, M.; Ullah, M. A.; Adeel, M.; Usman Khan, M.; Tahir, M. N.; Braga, A. A. C. Synthesis, Crystal Structure Analysis, Spectral IR, UV−Vis, NMR Assessments, Electronic and Nonlinear Optical Properties of Potent Quinoline Based Derivatives: Interplay of Experimental and DFT Study. *J. Saudi Chem. Soc.* **2019**, *23* (5), 546−560.

(21) Khalid, M.; Ali, A.; Khan, M. U.; Tahir, M. N.; Ahmad, A.; Ashfaq, M.; Hussain, R.; de Alcantara Morais, S. F.; Braga, A. A. C. Non-Covalent Interactions Abetted Supramolecular Arrangements of N-Substituted Benzylidene Acetohydrazide to Direct Its Solid-State Network. *J. Mol. Struct.* **2021**, *1230*, 129827.

(22) Parr, R. G.; Donnelly, R. A.; Levy, M.; Palke, W. E. Electronegativity: The Density Functional Viewpoint. *J. Chem. Phys.* **1978**, *68* (8), 3801−3807.

(23) Parr, R. G.; Szentpály, L. v; Liu, S. Electrophilicity Index. *J. Am. Chem. Soc.* **1999**, *121* (9), 1922−1924.

(24) Chattaraj, P. K.; Roy, D. R. Update 1 of: Electrophilicity Index. *Chem. Rev.* **2007**, *107* (9), PR46−PR74.

(25) Pettiette, C. L. *Studies of Copper, Silver, and Gold Cluster Anions: Evidence of Electronic Shell Structure*; Rice University, 1988.

(26) Ghiasuddin; Akram, M.; Adeel, M.; Khalid, M.; Tahir, M. N.; Khan, M. U.; Asghar, M. A.; Ullah, M. A.; Iqbal, M. A Combined Experimental and Computational Study of 3-Bromo-5-(2, 5-Difluorophenyl) Pyridine and 3, 5-Bis (Naphthalen-1-Yl) Pyridine: Insight into the Synthesis, Spectroscopic, Single Crystal XRD, Electronic, Nonlinear Optical and Biological Properties. *J. Mol. Struct.* **2018**, *1160*, 129−141.

(27) Aihara, J. Reduced HOMO- LUMO Gap as an Index of Kinetic Stability for Polycyclic Aromatic Hydrocarbons. *J. Phys. Chem. A* **1999**, *103* (37), 7487−7495.

(28) Ahmad, M. S.; Khalid, M.; Shaheen, M. A.; Tahir, M. N.; Khan, M. U.; Braga, A. A. C.; Shad, H. A. Synthesis and XRD, FT-IR Vibrational, UV−Vis, and Nonlinear Optical Exploration of Novel Tetra Substituted Imidazole Derivatives: A Synergistic Experimental-Computational Analysis. *J. Phys. Chem. Solids* **2018**, *115*, 265−276.

(29) Khalid, M.; Ali, A.; Jawaria, R.; Asghar, M. A.; Asim, S.; Khan, M. U.; Hussain, R.; Fayyaz ur Rehman, M.; Ennis, C. J.; Akram, M. S. First Principles Study of Electronic and Nonlinear Optical Properties of A−D−π−A and D−A−D−π−A Configured Compounds Containing Novel Quinoline−Carbazole Derivatives. *RSC Adv.* **2020**, *10* (37), 22273−22283.

(30) James, C.; Raj, A. A.; Reghunathan, R.; Jayakumar, V. S.; Joe, I. H. Structural Conformation and Vibrational Spectroscopic Studies of 2, 6-Bis (p-N, N-Dimethyl Benzylidene) Cyclohexanone Using Density Functional Theory. *J. Raman Spectrosc.* **2006**, *37* (12), 1381−1392.

(31) Szafran, M.; Komasa, A.; Bartoszak-Adamska, E. Crystal and Molecular Structure of 4-Carboxypiperidinium Chloride (4-Piperidinecarboxylic Acid Hydrochloride). *J. Mol. Struct.* **2007**, *827* (1−3), 101−107.

https://doi.org/10.1021/acsomega.2c02805
ACS Omega 2022, 7, 31036−31046

(32) Naseem, S.; Khalid, M.; Tahir, M. N.; Halim, M. A.; Braga, A. A.; Naseer, M. M.; Shafiq, Z. Synthesis, Structural, DFT Studies, Docking and Antibacterial Activity of a Xanthene Based Hydrazone Ligand. *J. Mol. Struct.* **2017**, *1143*, 235−244.
(33) Subashchandrabose, S.; Krishnan, A. R.; Saleem, H.; Parameswari, R.; Sundaraganesan, N.; Thanikachalam, V.; Manikandan, G. Vibrational Spectroscopic Study and NBO Analysis on Bis (4-Amino-5-Mercapto-1, 2, 4-Triazol-3-Yl) Methane Using DFT Method. *Spectrochim. Acta. A. Mol. Biomol. Spectrosc.* **2010**, *77* (4), 877−884.
(34) James, C.; Raj, A. A.; Reghunathan, R.; Jayakumar, V. S.; Joe, I. H. Structural Conformation and Vibrational Spectroscopic Studies of 2, 6-Bis (p-N, N-Dimethyl Benzylidene) Cyclohexanone Using Density Functional Theory. *J. Raman Spectrosc.* **2006**, *37* (12), 1381−1392.
(35) Khan, M. U.; Khalid, M.; Shafiq, I.; Khera, R. A.; Shafiq, Z.; Jawaria, R.; Shafiq, M.; Alam, M. M.; Braga, A. A. C.; Imran, M.; Kanwal, F.; Xu, Z.; Lu, C. Theoretical Investigation of Nonlinear Optical Behavior for Rod and T-Shaped Phenothiazine Based D-π-A Organic Compounds and Their Derivatives. *J. Saudi Chem. Soc.* **2021**, *25* (10), 101339.
(36) Khalid, M.; Shafiq, I.; Zhu, M.; Khan, M. U.; Shafiq, Z.; Iqbal, J.; Alam, M. M.; Braga, A. A. C.; Imran, M. Efficient Tuning of Small Acceptor Chromophores with A1-π-A2-π-A1 Configuration for High Efficacy of Organic Solar Cells via End Group Manipulation. *J. Saudi Chem. Soc.* **2021**, *25* (8), 101305.
(37) Adant, C.; Dupuis, M.; Bredas, J. L. Ab Initio Study of the Nonlinear Optical Properties of Urea: Electron Correlation and Dispersion Effects. *Int. J. Quantum Chem.* **1995**, *56* (S29), 497−507.
(38) Elhenawy, A. A.; Al-Harbi, L. M.; El-Gazzar, M. A.; Khowdiary, M. M.; Moustfa, A. Synthesis, Molecular Properties and Comparative Docking and QSAR of New 2-(7-Hydroxy-2-Oxo-2H-Chromen-4-Yl) Acetic Acid Derivatives as Possible Anticancer Agents. *Spectrochim. Acta. A. Mol. Biomol. Spectrosc.* **2019**, *218*, 248−262.
(39) Xu, L.; Zhang, J.; Yin, L.; Long, X.; Zhang, W.; Zhang, Q. Recent Progress in Efficient Organic Two-Photon Dyes for Fluorescence Imaging and Photodynamic Therapy. *J. Mater. Chem. C* **2020**, *8* (19), 6342−6349.
(40) Liang, X.; Zhang, Q. Recent Progress on Intramolecular Charge-Transfer Compounds as Photoelectric Active Materials. *Sci. China Mater.* **2017**, *60* (11), 1093−1101.
(41) Khan, M. U.; Khalid, M.; Shafiq, I.; Khera, R. A.; Shafiq, Z.; Jawaria, R.; Shafiq, M.; Alam, M. M.; Braga, A. A. C.; Imran, M.; Kanwal, F.; Xu, Z.; Lu, C. Theoretical Investigation of Nonlinear Optical Behavior for Rod and T-Shaped Phenothiazine Based D-Pi-A Organic Compounds and Their Derivative. *J. Saudi Chem. Soc.* **2021**, *25* (10), 101339.
(42) Qin, C.; Clark, A. E. DFT Characterization of the Optical and Redox Properties of Natural Pigments Relevant to Dye-Sensitized Solar Cells. *Chem. Phys. Lett.* **2007**, *438* (1−3), 26−30.
(43) Khalid, M.; Arshad, M. N.; Murtaza, S.; Shafiq, I.; Haroon, M.; Asiri, A. M.; de AlcântaraMorais, S. F.; Braga, A. A. Enriching NLO Efficacy via Designing Non-Fullerene Molecules with the Modification of Acceptor Moieties into ICIF2F: An Emerging Theoretical Approach. *RSC Adv.* **2022**, *12* (21), 13412−13427.
(44) Mulliken, R. S. Electronic Population Analysis on LCAO−MO Molecular Wave Functions. *Int. J. Chem. Phys.* **1955**, *23*, 1833−1840.
(45) Parr, R. G.; Pearson, R. G. Absolute Hardness: Companion Parameter to Absolute Electronegativity. *J. Am. Chem. Soc.* **1983**, *105* (26), 7512−7516.
(46) Li, L.; Wu, C.; Wang, Z.; Zhao, L.; Li, Z.; Sun, C.; Sun, T. Density Functional Theory (DFT) and Natural Bond Orbital (NBO) Study of Vibrational Spectra and Intramolecular Hydrogen Bond Interaction of l-Ornithine−l-Aspartate. *Spectrochim. Acta. A. Mol. Biomol. Spectrosc.* **2015**, *136*, 338−346.
(47) Burrows, J. A.; Pauling, L. *The Nature of the Chemical Bond and the Structure of Molecules Aid Crystals*; The Cornell University Press: Ithaca, NY, **1939**
(48) Frisch, M. J.; Trucks, G. W.; Schlegel, H. B.; Scuseria, G. E.; Robb, M. A.; Cheeseman, J. R.; Scalmani, G.; Barone, V.; Mennucci, B.; Petersson, G. A.; Nakatsuji, H.; Caricato, M.; Li, X.; Hratchian, H. P.; Izmaylov, A. F.; Bloino, J.; Zheng, G.; Sonnenberg, J. L.; Hada, M.; Ehara, M.; Toyota, K.; Fukuda, R.; Hasegawa, J.; Ishida, M.; Nakajima, T.; Honda, Y.; Kitao, O.; Nakai, H.; Vreven, T.; Montgomery, J. A., Jr.; Peralta, J. E.; Ogliaro, F.; Bearpark, M.; Heyd, J. J.; Brothers, E.; Kudin, K. N.; Staroverov, V. N.; Kobayashi, R.; Normand, J.; Raghavachari, K.; Rendell, A.; Burant, J. C.; Iyengar, S. S.; Tomasi, J.; Cossi, M.; Rega, N.; Millam, N. J.; Klene, M.; Knox, J. E.; Cross, J. B.; Bakken, V.; Adamo, C.; Jaramillo, J.; Gomperts, R.; Stratmann, R. E.; Yazyev, O.; Austin, A. J.; Cammi, R.; Pomelli, C.; Ochterski, J. W.; Martin, R. L.; Morokuma, K.; Zakrzewski, V. G.; Voth, G. A.; Salvador, P.; Dannenberg, J. J.; Dapprich, S.; Daniels, A. D.; Farkas, Ö.; Foresman, J. B.; Ortiz, J. V.; Cioslowski, J.; Fox, D. J. *Gaussian 09*; Gaussian, Inc.: Wallingford, CT, 2009.
(49) Hanwell, M. D.; Curtis, D. E.; Lonie, D. C.; Vandermeersch, T.; Zurek, E.; Hutchison, G. R. Avogadro: An Advanced Semantic Chemical Editor, Visualization, and Analysis Platform. *J. Cheminformatics* **2012**, *4* (1), 17.
(50) Dennington, R.; Keith, T.; Millam, J. G. *GaussView*; Semichem. Inc: Shawnee Mission, KS, 2009.
(51) Chatterjee, M.; Mondal, S.; Ghosh, P.; Kaim, W.; Lahiri, G. K. Mononuclear and Dinuclear Ruthenium Complexes of Cis-and Trans-Thioindigo: Geometrical and Electronic Structure Analyses. *Inorg. Chem.* **2018**, *57* (19), 12187−12194.
(52) Weinhold, F.; Glendening, E. D. *NBO 5.0 Program Manual: Natural Bond Orbital Analysis Programs*; Board of Regents of the University of Wisconsin: Madison, WI, 2001.
(53) Khan, I.; Khalid, M.; Adeel, M.; Niaz, S. I.; Shafiq, I.; Muhammad, S.; Braga, A. A. C. Palladium-Catalyzed Synthesis of 5-(Arylated) Pyrimidines, Their Characterization, Electronic Communication, and Non-Linear Optical Evaluations. *J. Mol. Struct.* **2021**, *1237*, 130408.
(54) Muthu, S.; Ramachandran, G. Spectroscopic Studies (FTIR, FT-Raman and UV−Visible), Normal Coordinate Analysis, NBO Analysis, First Order Hyper Polarizability, HOMO and LUMO Analysis of (1R)-N-(Prop-2-Yn-1-Yl)-2, 3-Dihydro-1H-Inden-1-Amine Molecule by Ab Initio HF and Density Functional Methods. *Spectrochim. Acta. A. Mol. Biomol. Spectrosc.* **2014**, *121*, 394−403.
(55) Fukui, K. Role of Frontier Orbitals in Chemical Reactions. *science* **1982**, *218* (4574), 747−754.
(56) Breitung, E. M.; Shu, C.-F.; McMahon, R. J. Thiazole and Thiophene Analogues of Donor- Acceptor Stilbenes: Molecular Hyperpolarizabilities and Structure- Property Relationships. *J. Am. Chem. Soc.* **2000**, *122* (6), 1154−1160.

https://doi.org/10.1021/acsomega.2c02805
ACS Omega 2022, 7, 31036−31046